Journal of Power Sources 263 (2014) 280–287

Contents lists available at ScienceDirect

Journal of Power Sources

journal homepage: www.elsevier.com/locate/jpowsour

Preparation of ternary Pt/Rh/SnO_2 anode catalysts for use in direct ethanol fuel cells and their electrocatalytic activity for ethanol oxidation reaction

Eiji Higuchi*, Tomonori Takase, Masanobu Chiku, Hiroshi Inoue*

Department of Applied Chemistry, Graduate School of Engineering, Osaka Prefecture University, Sakai, Osaka 599-8531, Japan

HIGHLIGHTS

- Ternary Pt/Rh/SnO_2 catalysts can be prepared by the modified Bönnemann method.
- Pt and Rh components were metallic and Sn component was oxidized to SnO_2.
- Each Pt/Rh/SnO_2/CB catalyst was composed of Pt, Rh and/or SnO_2 nanoparticles.
- EOR activity of Pt-65/Rh-10/SnO_2/CB is higher than that of Pt/SnO_2/CB.
- EOR at 0.6 V for Pt/Rh/SnO_2/CB decayed more slowly than that at the Pt/SnO_2/CB.

ARTICLE INFO

Article history:
Received 3 March 2014
Received in revised form
9 April 2014
Accepted 11 April 2014
Available online 24 April 2014

Keywords:
Pt/Rh/SnO_2/CB
Ethanol oxidation
Electrocatalyst
Nanoparticle

ABSTRACT

Pt, Rh and SnO_2 nanoparticle-loaded carbon black (Pt/Rh/SnO_2/CB) catalysts with different contents of Pt and Rh were prepared by the modified Bönnemann method. The mean size and size distribution of Pt, Rh and SnO_2 for Pt-71/Rh-4/SnO_2/CB (Pt : Rh : Sn = 71 at.%: 4 at.%: 25 at.%) were 3.8 ± 0.7, 3.2 ± 0.7 and 2.6 ± 0.5 nm, respectively, indicating that Pt, Rh and SnO_2 were all nanoparticles. The onset potential of ethanol oxidation current for the Pt-65/Rh-10/SnO_2/CB and Pt-56/Rh-19/SnO_2/CB electrodes was ca. 0.2 V vs. RHE which was ca. 0.2 V less positive than that for the Pt/CB electrode. The oxidation current at 0.6 V for the Pt/Rh/SnO_2/CB electrode (ca. 2% h^{-1}) decayed more slowly than that at the Pt/SnO_2/CB electrode (ca. 5% h^{-1}), indicating that the former was superior in durability to the latter. The main product of EOR in potentiostatic electrolysis at 0.6 V for the Pt-71/Rh-4/SnO_2/CB electrode was acetic acid.

1. Introduction

Direct ethanol fuel cells (DEFCs) have attracted much interest as a primary power source for portable electronic devices. Ethanol is a nontoxic fuel that can be easily produced in large quantity by carbon-neutral processes. Ethanol oxidation reaction (EOR) at the anode ideally produces CO_2 as represented by the following equation [1–3].

$$C_2H_5OH + 3H_2O \rightarrow 2CO_2 + 12H^+ + 12e^- \quad (1)$$

However, this reaction is hard to proceed because of the difficulty in breaking the C–C bond of an ethanol molecule. Consequently, some byproducts such as acetic acid and acetaldehyde are mainly produced. Therefore, the development of electrocatalysts which can break the C–C bond is an urgent issue [4–7].

So far there have been many reports on the development of binary and ternary electrocatalysts in order to enhance the EOR activity [4,8–20]. In particular, it is known that binary PtSn catalysts have high EOR activity [1–6]. We also prepared the Pt/SnO_2 double nanoparticles-loaded carbon black (Pt/SnO_2/CB) by using the modified Bönnemann method, and found it exhibited higher EOR activity than the Pt nanoparticles-loaded CB [16,21]. In particular, the Pt/SnO_2(3:1)/CB (Pt : Sn = 3 : 1 in atomic ratio) electrode exhibited the highest EOR activity per real surface area of Pt [16,21]. However, in this case acetic acid was the main product. So the addition of the third element to PtSn must be required to break the C–C bond. It has been reported that the addition of Rh to the Pt–SnO_2/C or PtSn/C electrocatalysts increased the CO_2 selectivity and/or improved the EOR activity [4,22–24]. In particular,

* Corresponding authors. Tel./fax: +81 72 254 9319.
E-mail address: e-higuchi@chem.osakafu-u.ac.jp (E. Higuchi).

http://dx.doi.org/10.1016/j.jpowsour.2014.04.056
0378-7753/

Kowal et al. reported that ternary Pt–Rh–SnO_2 catalyst was effective for the oxidation of ethanol to CO_2 by synergy effect between the Pt, Rh and SnO_2 and the addition of Rh to Pt–SnO_2 catalyst promote a direct breaking of the C–C bond using density functional theory calculation [4]. So the addition of a third element like Rh into the Pt/SnO_2(3:1)/CB catalyst we prepared may enable a complete EOR to CO_2. If ternary catalysts of Pt, Rh and SnO_2 are prepared by our method, they may realize complete EOR to CO_2 with maintaining its high EOR activity. In the case of such ternary catalysts, understanding of the role of each constituent is needed for obtaining the high electrocatalytic activity. In this study, in order to confirm this hypothesis we prepared ternary nanoparticle catalysts which consist of Pt, Rh and SnO_2 by the modified Bönnemann method. In addition, EOR activity and durability for the Pt/Rh/SnO_2/CB catalysts were evaluated.

2. Experimental

2.1. Preparation of Pt/Rh/SnO_2/CB and Pt/SnO_2/CB catalysts

$N(Oct)_4BEt_3H$ (Oct: $-C_8H_{17}$, Et: $-C_2H_5$) as a reducing agent was prepared according to Ref. [25]. To prepare a Pt/Rh/SnO_2 ((Pt + Rh):Sn = 75 : 25 in mol. %) catalyst, a solution of 0.3 M $N(Oct)_4(BEt_3H)$ in tetrahydrofuran (THF, 13.6 mL, Wako Pure Chemical Industries, Ltd.) was added dropwise to a vigorously stirred solution containing $PtCl_2$ (0.71 mmol, Wako Pure Chemical), $RhCl_3 \cdot 3H_2O$ (0.04 mmol) and $SnCl_2$ (0.25 mmol, Wako Pure Chemical) at 50 °C in an Ar atmosphere, and then the mixture was still stirred for 5 h, resulting in a black colloidal suspension. To oxidize any excess $N(Oct)_4(BEt_3H)$, acetone (15 mL) was added into the suspension, followed by stirring for 30 min. The black colloidal suspension was isolated by suction filtration in air and dried in vacuum at room temperature for 16 h, yielding a black, waxy solid. Exposure to air during the filtration caused the oxidation of Sn.

The black solid was redispersed in ethanol. An appropriate amount of Ketjen Black (Ketjenblack International Co., EC300J) was added in the dispersion and sonicated for 1 h. After suction filtration, a residual black powder was collected and heat-treated at 250 °C in air for 30 min to remove $N(Oct)_4Cl$. The resultant powder was called Pt-71/Rh-4/SnO_2/CB in which the contents of Pt, Rh and SnO_2 were 71, 4 and 25 mol%, respectively. Total content of Pt, Rh and SnO_2 in the Pt/Rh/SnO_2/CB is *ca.* 70 wt. %.

Pt-65/Rh-10/SnO_2/CB (Pt : Rh : Sn = 65 : 10 : 25 in mol%) and Pt-56/Rh-19/SnO_2/CB (Pt : Rh : Sn = 56 : 19 : 25 in mol%) powders were also prepared by the same procedure although the amount of $PtCl_2$ and $RhCl_3$ was changed to 0.65 and 0.10 mmol and 0.56 and 0.19 mmol, respectively.

2.2. Characterization of Pt/Rh/SnO_2/CB and Pt/SnO_2/CB catalysts

Thermogravimetric (TG) analysis was performed in air using a Thermo Plus TG8120 apparatus (Rigaku) by heating from room temperature to 500 °C at a rate of 1 K min^{-1}. Microstructure of Pt-71/Rh-4/SnO_2/CB, Pt-65/Rh-10/SnO_2/CB and Pt-56/Rh-19/SnO_2/CB was examined by field-emission transmission electron microscopy (FE-TEM, HF-2000, Hitachi). FE-TEM specimens were prepared by casting a drop of an ethanol dispersion of each catalyst onto a collodion-coated Cu grid and evaporating ethanol. Size distribution of Pt, Rh and SnO_2 nanoparticles was measured for 500 Pt, 100 Rh and 100 SnO_2 nanoparticles randomly chosen from high resolution TEM images. Structural analysis for Pt-71/Rh-4/SnO_2/CB, Pt-65/Rh-10/SnO_2/CB and Pt-56/Rh-19/SnO_2/CB catalysts was performed using an X-ray diffractometer (Shimadzu XRD-6100, 50 kV, 30 mA) equipped with a CuKα source ($\lambda = 0.1541$ nm). Chemical states of Pt, Rh and Sn in each catalyst were characterized by X-ray photoelectron spectroscopy (XPS) using a photoelectron spectrometer (ESCA-3200, Shimadzu). The X-ray source was MgKα with 1253.6 eV operating at 8 kV and 30 mA. The base pressure of the system was 5.0×10^{-6} Pa. The content in at. % of Pt, Rh and Sn of Pt-71/Rh-4/SnO_2/CB, Pt-65/Rh-10/SnO_2/CB and Pt-56/Rh-19/SnO_2/CB catalysts was estimated by energy dispersive X-ray analysis (EDX, VE-9800, KEYENCE).

2.3. Electrochemical measurements

The Pt-71/Rh-4/SnO_2/CB, Pt-65/Rh-10/SnO_2/CB and Pt-56/Rh-19/SnO_2/CB catalysts were cast on a glassy carbon (GC) substrate of ϕ5 mm according to the previous method [16]. The amount of Pt-71/Rh-4/SnO_2/CB, Pt-65/Rh-10/SnO_2/CB and Pt-56/Rh-19/SnO_2/CB catalysts in their suspensions was adjusted to $w_{CB} = 5.5$ μg cm^{-2} (w_{CB}: amount of CB loaded on GC). The amount of Pt/Rh/SnO_2 loaded on the GC ($w_{Pt/Rh/SnO2}$) was 12.8 μg cm^{-2}. A 0.05 wt.% Nafion solution (Aldrich) in ethanol (10 μL) was cast on the dried catalyst layer, and then dried in air at 120 °C for 1 h, resulting in a catalyst electrode coated with a thin Nafion film of 0.1 μm. A glass cell was used for electrochemical characterization of the Pt-71/Rh-4/SnO_2/CB, Pt-65/Rh-10/SnO_2/CB and Pt-56/Rh-19/SnO_2/CB electrodes. A Pt plate and a reversible hydrogen electrode (RHE) were used as the counter and reference electrodes, respectively. EOR activity and durability of each electrode were evaluated at 30 °C by cyclic voltammetry and potentiostatic electrolysis, respectively. In CO-stripping voltammetry, CO was adsorbed on each electrode by immersing in a 0.1 M $HClO_4$ solution saturated with CO for 15 min at a constant potential of 0.05 V vs. RHE. The excess CO was eliminated by Ar bubbling. The stripping voltammogram was measured from 0.05 to 1.0 V vs. RHE at a sweep rate of 50 mV s^{-1}.

2.4. Qualitative and quantitative analyses of reaction products in potentiostatic electrolyses

Products in potentiostatic electrolyses with the Pt-71/Rh-4/SnO_2/CB, Pt-65/Rh-10/SnO_2/CB and Pt-56/Rh-19/SnO_2/CB electrodes were qualitatively and quantitatively analyzed by a high performance liquid chromatograph (HPLC, Tosoh) equipped with an UV detector (UV-8020) for acetic acid and acetaldehyde and a gas chromatograph (GC, Shimadzu GC-14B) for CO_2.

3. Results and discussion

3.1. Structures of Pt-71/Rh-4/SnO_2/CB, Pt-65/Rh-10/SnO_2/CB and Pt-56/Rh-19/SnO_2/CB catalysts

The bulk contents of Pt, Rh and Sn in Pt-71/Rh-4/SnO_2/CB, Pt-65/Rh-10/SnO_2/CB and Pt-56/Rh-19/SnO_2/CB were evaluated by EDX and summarized in Table 1. The contents of Pt, Rh and Sn in each catalyst were nearly equal to those in the mixed Pt, Rh and Sn precursor solutions. Thus bulk compositions of these Pt/Rh/SnO_2/CB catalysts can be controlled by those of the mixed precursor solutions.

Table 1
Bulk compositions of Pt/Rh/SnO_2/CB catalysts.

Catalyst	Pt : Rh : Sn/at. %	
	Theoretical	Experimental
Pt-71/Rh-4/SnO_2/CB	71 : 4 : 25	72 : 4 : 24
Pt-65/Rh-10/SnO_2/CB	65 : 10 : 25	67 : 12 : 21
Pt-56/Rh-19/SnO_2/CB	56 : 19 : 25	59 : 19 : 22

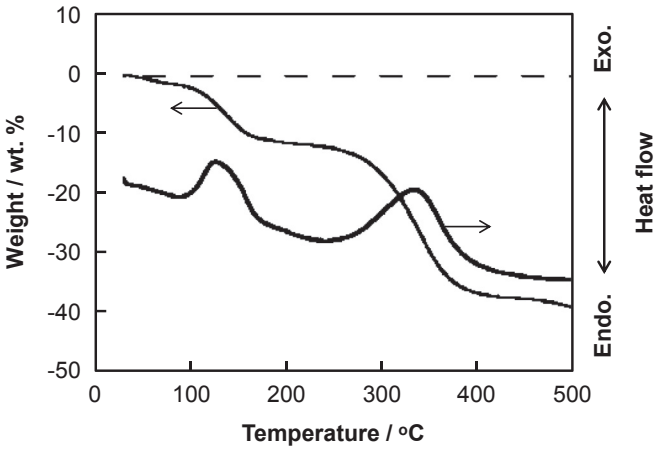

Fig. 1. TG-DTA curves of as-prepared Pt-71/Rh-4/SnO_2/CB.

Fig. 1 shows TG–DTA curves for as-prepared Pt-71/Rh-4/SnO_2/CB catalyst. The initial weight loss below 100 °C (*ca.* 3 wt. %) was assigned to evaporation of physisorbed water from the as-prepared Pt-71/Rh-4/SnO_2/CB and the second weight loss observed between 100 and 200 °C is due to oxidation of the stabilizer $N(Oct)_4Cl$; this is in agreement with some previous reports [16,26]. The oxidation of CB started at about 250 °C. Consequently, weight losses due to the oxidation of $N(Oct)_4Cl$ and CB were *ca.* 9 wt. % and *ca.* 27 wt. %, respectively. Therefore, total content of Pt, Rh and SnO_2 loaded in Pt-71/Rh-4/SnO_2/CB catalysts was evaluated to be *ca.* 69 wt. %.

Fig. 2 shows FE-TEM images of Pt-71/Rh-4/SnO_2/CB, Pt-65/Rh-10/SnO_2/CB and Pt-56/Rh-19/SnO_2/CB catalysts. Fig. 2(a), (b) and 2(c) clearly show the production of nanoparticles on CB. Fig. 2(d) shows a high resolution TEM image of the Pt-71/Rh-4/SnO_2/CB catalyst. In this figure, three kinds of lattice fringes with interfringe distances of 0.23, 0.22 and 0.33 nm were observed. These lattice fringes were in close agreement with those of the Pt(111) plane

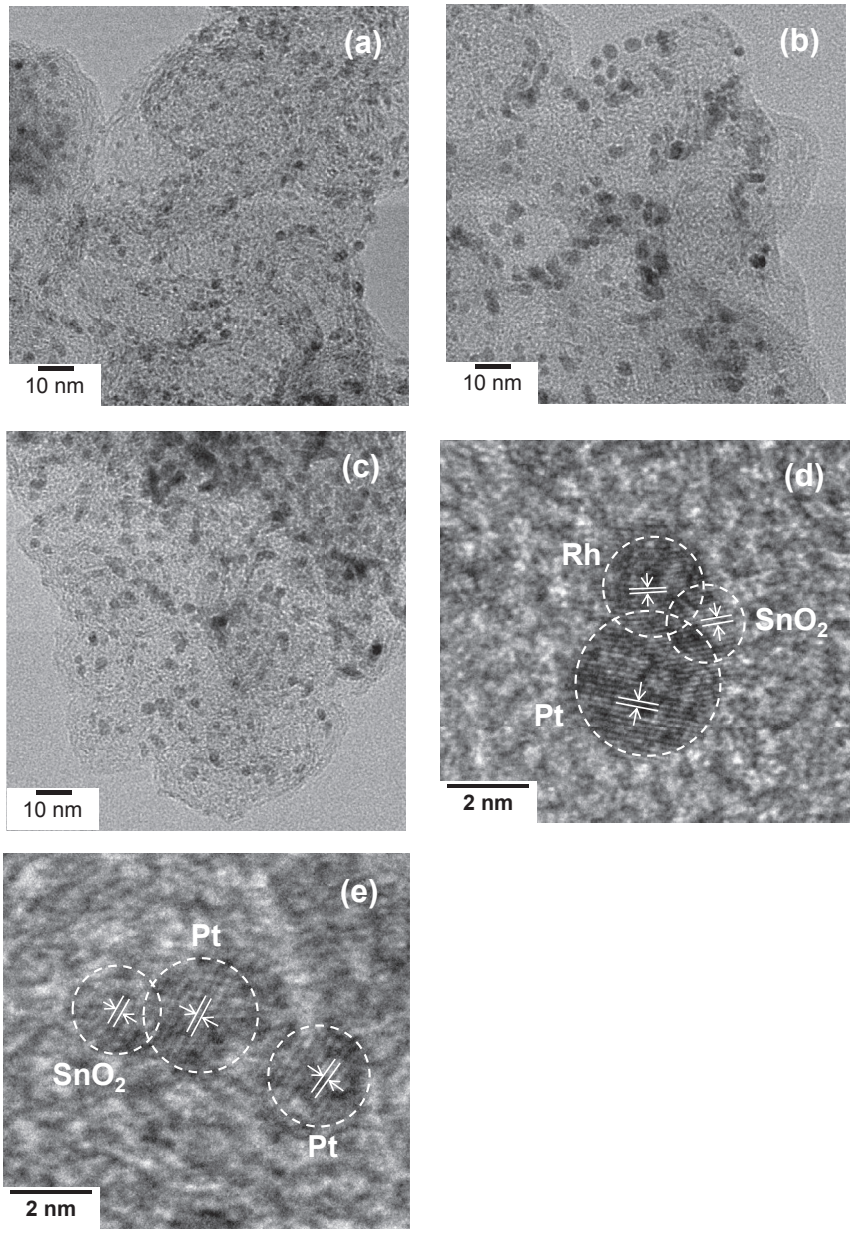

Fig. 2. TEM images of (a) Pt-71/Rh-4/SnO_2/CB (b) Pt-65/Rh-10/SnO_2/CB and (c) Pt-56/Rh-19/SnO_2/CB. The (d) and (e) is a high resolution TEM image of (a).

(0.227 nm), the Rh(111) plane (0.220 nm), and the SnO_2(110) plane (0.335 nm), respectively. The Pt, Rh and SnO_2 nanoparticles were partially contact with each other as shown in Fig. 2(d), and a fraction of binary and single nanoparticles were also observed like Fig. 2(e).

Fig. 3 shows particle size distribution profiles of Pt, Rh and SnO_2 particles for Pt-71/Rh-4/SnO_2/CB, Pt-65/Rh-10/SnO_2/CB and Pt-56/Rh-19/SnO_2/CB. Mean particle size and standard deviation of the Pt, Rh and SnO_2 nanoparticles were summarized in Table 2. The mean particle size of the Rh nanoparticles seems to a little bit depended on the Rh content, while that of the Pt and SnO_2 nanoparticles was not influenced by catalyst composition.

Fig. 4 shows XRD patterns of Pt-71/Rh-4/SnO_2/CB, Pt-65/Rh-10/SnO_2/CB, Pt-56/Rh-19/SnO_2/CB and SnO_2/CB catalysts. Each XRD pattern had diffraction peaks at 39.8, 46.2, 67.4, 81.3 and 85.7° which were assigned to Pt(111), (200), (220), (311) and (222), respectively. These are characteristic of the face centered cubic (fcc) structure. On the other hand, peaks at 41.1 and 47.8° were assigned to Rh(111) and Rh(200), respectively. And, the Rh was cubic structure. The lattice constant of Pt and Rh evaluated with the (111) peak was 0.393 and 0.380 nm irrespective of catalyst composition, which was in good agreement with the lattice constant of Pt (0.3923 nm) and Rh (0.3803 nm). On the other hand, diffraction peaks at 26.6°, 33.9° and 51.8 °for SnO_2/CB were assigned to SnO_2(110), (101), and (211), respectively. These suggests that Pt does not form any alloy with Rh and Sn during the preparation of each catalyst. And the diffraction pattern of SnO_2 was very small because of small particle size (2 nm). For the Pt-56/Rh-19/SnO_2/CB catalyst, weak diffraction peaks assigned to SnO_2(110) and SnO_2(211) were observed at $2\theta = 26.6°$, 33.9° and 51.8°, respectively, because SnO_2 content was very low. Pt and Rh have very close diffraction peak positions due to their similar crystalline structure [27]. As a result of measurement with narrow region from $2\theta = 30°–50°$, weak diffraction peaks assigned to Rh(111) and Rh(200) were observed at $2\theta = 41.1°$ and 47.8°, respectively.

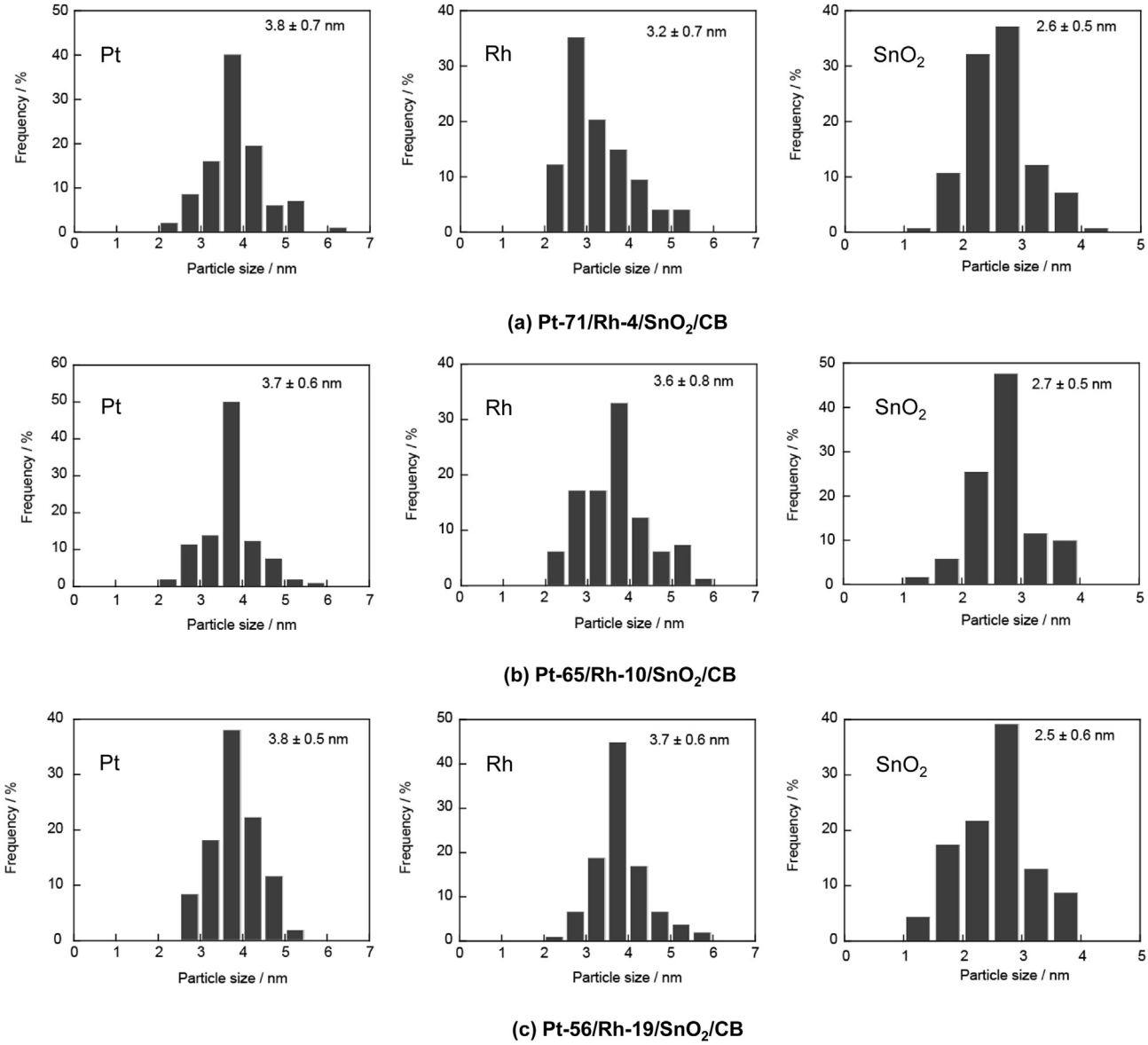

Fig. 3. Particle size distribution profiles of Pt, Rh and SnO_2 particles for (a) Pt-71/Rh-4/SnO_2/CB (b) Pt-65/Rh-10/SnO_2/CB and (c) Pt-56/Rh-19/SnO_2/CB.

Table 2
Mean particle size and size distribution of Pt/Rh/SnO_2/CB catalysts.

Catalysts	d_{XRD}/nm	d_{TEM}/nm		
	Pt	Pt	Rh	SnO_2
Pt-71/Rh-4/SnO_2-25/CB	4.2	3.8 ± 0.7	3.2 ± 0.7	2.6 ± 0.5
Pt-65/Rh-10/SnO_2-25/CB	3.9	3.7 ± 0.6	3.6 ± 0.8	2.7 ± 0.5
Pt-56/Rh-19/SnO_2-25/CB	3.8	3.8 ± 0.5	3.7 ± 0.6	2.5 ± 0.6
Pt-75/SnO_2/CB	3.4	3.1 ± 0.5	–	2.5 ± 0.3

Fig. 5 shows Pt4f, Rh3d and Sn3d core level spectra for the Pt-71/Rh-4/SnO_2/CB, Pt-65/Rh-10/SnO_2/CB and Pt-56/Rh-19/SnO_2/CB catalysts. A peak of 79.2 eV is $4f_{5/2}$ orbit of the Au which we used as a standard sample. The Pt4f spectra exhibited strong doublets at 71.1 eV ($4f_{7/2}$) and 74.4 eV ($4f_{5/2}$) (Fig. 5(a)), which were assigned to metallic Pt (Pt^0), but there were not any peaks assigned to Pt oxides. In contrast, the Rh3d spectra exhibited very weak doublets at 307.2 eV ($3d_{5/2}$) and 311.94 eV ($3d_{3/2}$) (Fig. 5(b)), which were assigned to metallic Rh (Rh^0). And these peaks became unclear with a decrease in Rh content. As for the Sn3d spectra (Fig. 5(c)), distinct strong doublets which were assigned to the $3d_{3/2}$ (495.1 eV) and $3d_{5/2}$ (486.7 eV) of Sn^{4+} were observed, but there were no doublets of metallic Sn (493.2 and 484.8 eV), suggesting that Sn was oxidized to SnO_2 during the preparation of each catalyst. In N1s and Cl2p core level spectra of all catalysts, there were no peaks, suggesting that $N(Oct)_4Cl$ as a stabilizer was completely removed during the heat-treatment.

3.2. Electrochemical properties and EOR activity of Pt/Rh/SnO_2/CB and Pt/SnO_2/CB electrodes

Fig. 6 shows cyclic voltammograms of Nafion-coated Pt-71/Rh-4/SnO_2/CB, Pt-65/Rh-10/SnO_2/CB, Pt-56/Rh-19/SnO_2/CB and Pt-75/SnO_2/CB electrodes in an Ar-saturated 0.1 M $HClO_4$ solution at 30 °C. A couple of redox peaks due to hydrogen adsorption and desorption on the Pt surface were observed in potentials less than 0.38 V vs. RHE in each CV [28]. The electrochemically active surface area (ECSA) of the Pt nanoparticles in each catalyst was evaluated from the electric charge for the hydrogen desorption wave, supposing 210 μC cm^{-2} for polycrystalline Pt. ECSA was 0.26, 0.22, 0.24 and 0.24 cm^2 for Pt-71/Rh-4/SnO_2/CB, Pt-65/Rh-10/SnO_2/CB, Pt-56/Rh-19/SnO_2/CB and Pt-75/SnO_2 electrodes, respectively.

Fig. 7(a) shows cyclic voltammograms (CVs) for the Pt-71/Rh-4/SnO_2/CB, Pt-65/Rh-10/SnO_2/CB, Pt-56/Rh-19/SnO_2/CB and Pt-75/SnO_2/CB electrodes in an Ar-saturated 0.1 M $HClO_4$ solution containing 1 M ethanol. In Fig. 7(b), current density (j) per ECSA of Pt was used in place of current. As can be seen from these figures, the onset potential of oxidation current for the Pt-75/SnO_2/CB electrode was ca. 0.2 V vs. RHE which was ca. 0.2 V less positive than that for the Pt/CB electrode (ca. 0.40 V vs. RHE [16]) because SnO_2 synergistically enhanced the EOR activity of Pt by the bifunctional mechanism [15,16,29,30] in which Sn atoms adjacent to Pt atoms supplied oxygen-containing species for the oxidative removal of Pt-bound CO-like intermediates. On the other hand, the onset potential for the Pt-65/Rh-10/SnO_2/CB and Pt-56/Rh-19/SnO_2/CB electrodes was also ca. 0.2 V vs. RHE which was ca. 0.2 V less positive

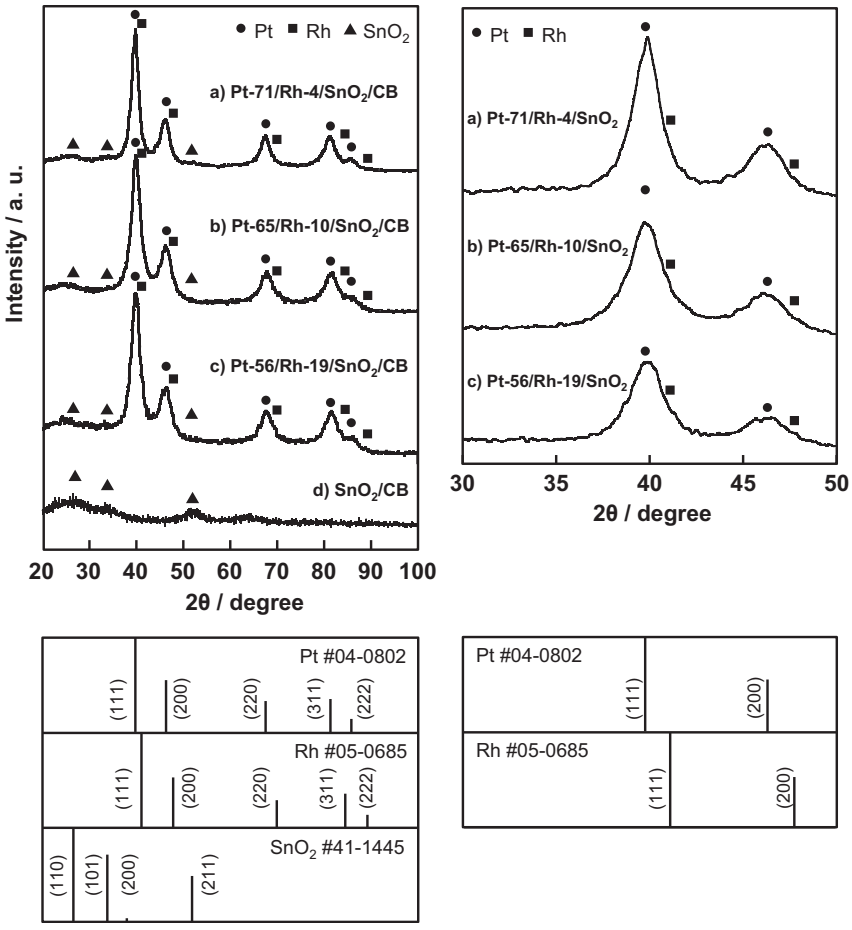

Fig. 4. XRD patterns of (a) Pt-71/Rh-4/SnO_2/CB, (b) Pt-65/Rh-10/SnO_2/CB, (c) Pt-56/Rh-19/SnO_2/CB and (d) SnO_2/CB catalysts.

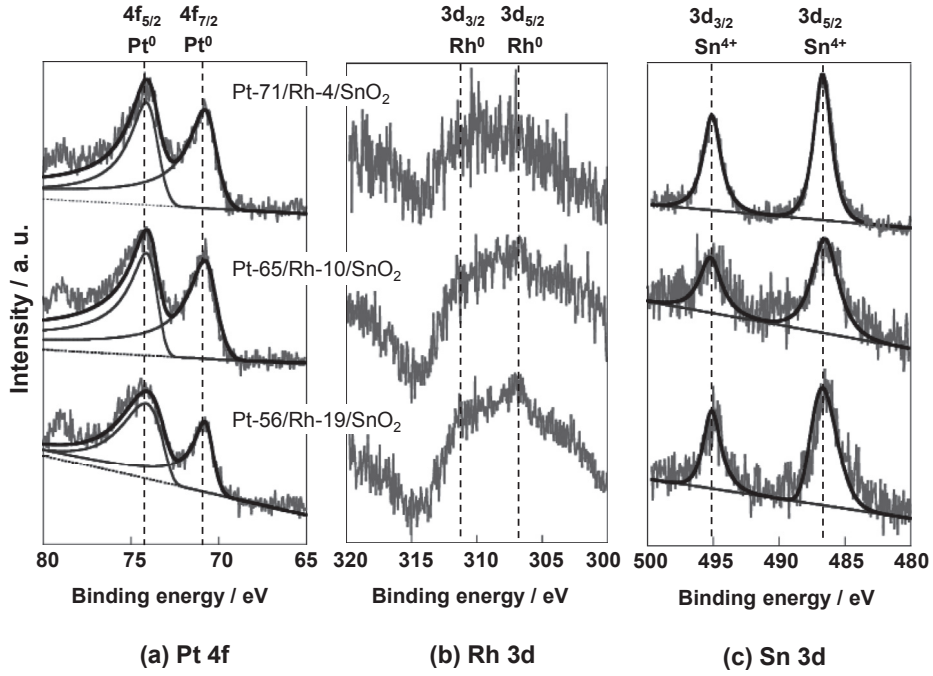

Fig. 5. (a) Pt4f, (b) Rh3d and (c) Sn3d core level spectra for Pt-71/Rh-4/SnO_2-25/CB, Pt-65/Rh-10/SnO_2-25/CB and Pt-56/Rh-19/SnO_2-25/CB catalysts.

than that for the Pt/CB electrode. In addition, as shown in Fig. 7(b), the Pt-65/Rh-10/SnO_2/CB electrodes showed highest EOR current density in this study. Not only the OER activity but also the selectivity of CO_2 production were improved for the Pt/Rh/SnO_2 electrodes.

Fig. 8 shows CO-stripping voltammograms of Pt-71/Rh-4/SnO_2/CB, Pt-65/Rh-10/SnO_2/CB, Pt-56/Rh-19/SnO_2/CB and Pt-75/SnO_2/CB electrodes. For the Pt-75/SnO_2/CB electrode, the onset potential of CO stripping was ca. 0.25 V, and the stripping peak was composed of a shoulder at the lower potential (ca. 0.35 V) which was assigned to CO oxidation at Pt atoms adjacent to Sn atoms and a peak at the higher potential (ca. 0.8 V) which was assigned to CO oxidation at isolated Pt atoms [16]. For the three Pt/Rh/SnO_2/CB electrodes, the shoulder at the lower potential was shifted to more positive potentials, suggesting that SnO_2 sites adjacent to Pt atoms which

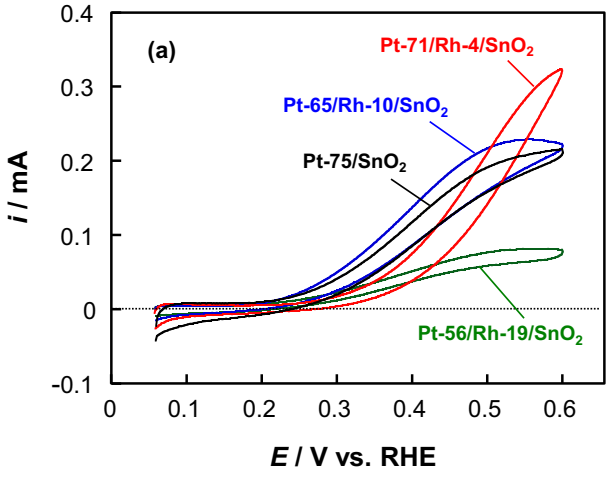

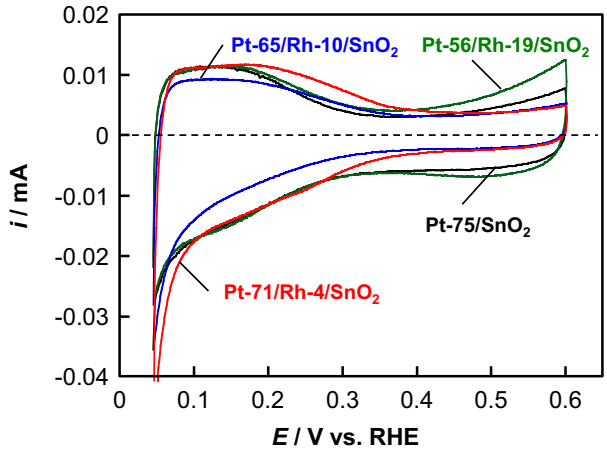

Fig. 6. CVs of Pt-71/Rh-4/SnO_2/CB, Pt-65/Rh-10/SnO_2/CB and Pt-56/Rh-19/SnO_2/CB, Pt-75/SnO_2/CB electrodes in an Ar-saturated 0.1 M $HClO_4$ solution at 30 °C. Sweep rate: 20 mV s^{-1}.

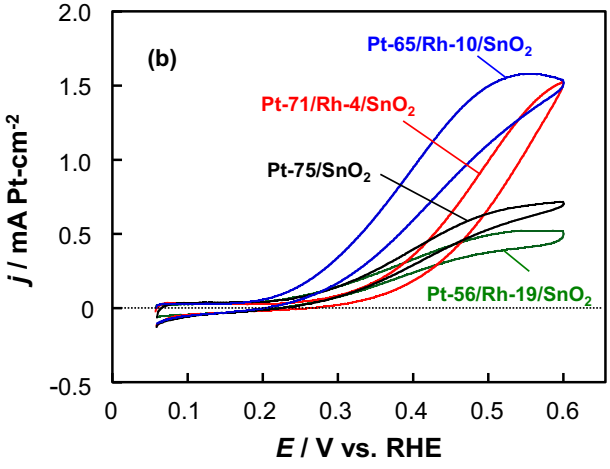

Fig. 7. CVs of Pt-71/Rh-4/SnO_2/CB, Pt-65/Rh-10/SnO_2/CB, Pt-56/Rh-19/SnO_2/CB and Pt-75/SnO_2/CB electrodes in Ar-saturated (1 M C_2H_5OH + 0.1 M $HClO_4$) solution at 30 °C. Sweep rate: 20 mV s^{-1}.

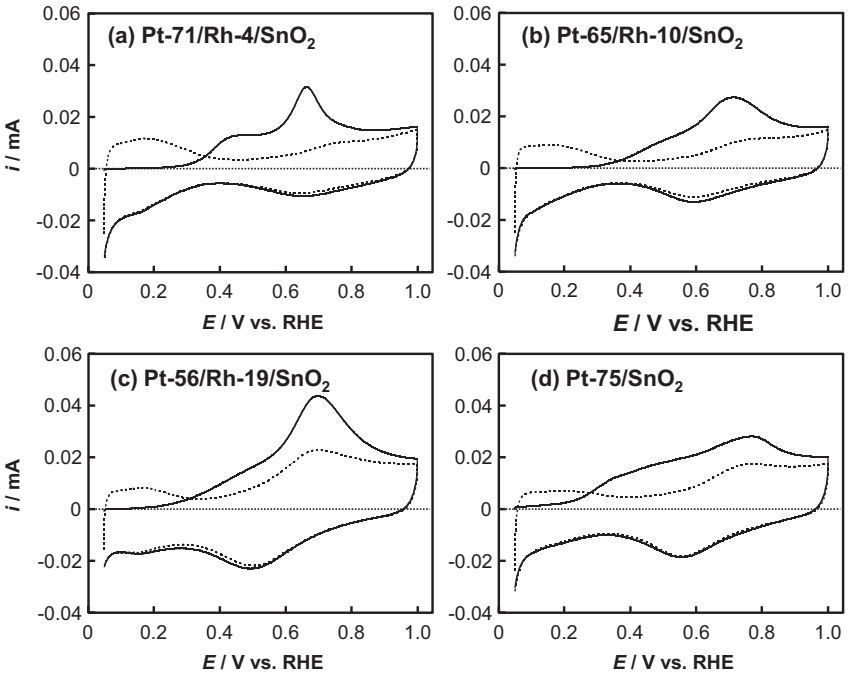

Fig. 8. CO-stripping voltammograms for the (a) Pt-71/Rh-4/SnO_2/CB, (b) Pt-65/Rh-10/SnO_2/CB, (c) Pt-56/Rh-19/SnO_2/CB and (d) Pt-75/SnO_2/CB catalysts in 0.1 M $HClO_4$ solution at 30 °C. Sweep rate: 50 mV s^{-1}.

caused the bifunctional effect were decreased. In contrast, the peak at the higher potential was shifted to the lower potentials with the addition of Rh. It is known that CO oxidation at isolated Rh atoms occurred at a lower potential than that at isolated Pt atoms [4]. So the addition of Rh causes the decrease in isolated Pt atoms and Pt atoms adjacent to Sn atoms or the increase in Rh atoms adjacent to Sn and Pt atoms.

The EOR activity of Pt/Rh/CB is similar to that of Pt/CB [23], indicating that Pt–Rh sites do not improve EOR activity. The EOR activity of Pt-65/Rh-10/SnO_2/CB electrode is higher than that of Pt/SnO_2/CB electrode, despite the fact that addition of Rh to Pt has no effect on the rate for EOR. Kowal et al. reported that SnO_2 by strongly adsorbing water and interacting with the Pt and Rh deposited on its surface, apparently precludes the Rh and Pt sites from reacting with H_2O to form M–OH (M = Pt, Rh), making them available for ethanol oxidation [4]. SnO_2 with H_2O provides OH species to oxidize the dissociated CO at Rh sites, and Pt facilitates ethanol dehydrogenation [4]. Thus, both SnO_2 and Rh at Pt are necessary for an active electrocatalyst.

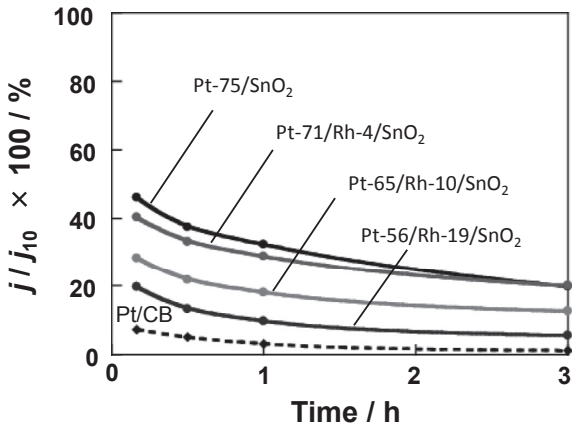

Fig. 9. Time courses of current density at 0.60 V for the Pt-71/Rh-4/SnO_2/CB, Pt-65/Rh-10/SnO_2/CB, Pt-56/Rh-19/SnO_2/CB, Pt-75/SnO_2CB and Pt/CB electrodes in Ar-saturated (1 M C_2H_5OH + 0.1 M $HClO_4$) solution at 30 °C. Sweep rate: 20 mV s^{-1}.

Fig. 9 shows time courses of standardized current density (j/j_{10}) for EOR at 0.6 V for Pt-71/Rh-4/SnO_2/CB, Pt-65/Rh-10/SnO_2/CB, Pt-56/Rh-19/SnO_2/CB, Pt-75/SnO_2/CB and Pt/CB electrodes in Ar-saturated (1 M C_2H_5OH + 0.1 M $HClO_4$) solutions at 30 °C. The j/j_{10} is defined as the percentage of current density per ECSA of Pt at 0.5, 1 or 3 h to that at 10 min. The decrement of oxidation current density for each Pt/Rh/SnO_2/CB electrode was ca. 2% h^{-1} irrespective of the Rh content, and it was smaller than that for the Pt-75/SnO_2/CB electrode (ca. 5% h^{-1}), indicating that each Pt/Rh/SnO_2/CB electrode was superior in durability to the Pt-75/SnO_2/CB electrode.

In potentiostatic electrolyses at 0.6 V for the Pt-71/Rh-4/SnO_2/CB, Pt-65/Rh-10/SnO_2/CB or Pt-56/Rh-19/SnO_2/CB electrode, acetic acid and CO_2 were produced, while acetaldehyde was not detected. Current efficiency for the production of acetic acid and CO_2 is summarized in Table 3. In all cases the predominant reaction product was acetic acid, which was the same as the case for the Pt-75/SnO_2/CB catalyst. This suggests that there are many numbers of the Pt–SnO_2 site. Surprisingly, the current density for CO_2 production of the Rh-containing catalysts was smaller than that of the Pt-75/SnO_2/CB catalyst although Kowal et al. reported that a ternary PtRhSnO_2/C catalyst significantly improved the CO_2 selectivity [4]. Main product of EOR for the Pt/SnO_2 electrode was acetic acid [31]. On the other hand, at the Pt/Rh electrode, the CO_2 was formed, while that of acetic acid was suppressed

Table 3
Current efficiency of EOR for Pt/Rh/SnO_2/CB and Pt/SnO_2/CB electrodes.

Catalyst	Applied potential	Current efficiency/%		
		Acetic acid	CO_2	Total
Pt-71/Rh-4/SnO_2/CB	0.6 V	85	10	95
Pt-65/Rh-10/SnO_2/CB	0.6 V	90	10	100
Pt-56/Rh-19/SnO_2/CB	0.6 V	80	10	90
Pt-75/SnO_2/CB	0.6 V	69	27	96

[31]. This indicates there is appropriate arrangement of Pt, Rh and SnO_2 atoms for CO_2 production. The understanding of the role of the Pt, Rh and SnO_2 components and their appropriate arrangement must be the key to the complete oxidation of ethanol to CO_2. Further studies are now in progress to investigate this idea.

4. Conclusions

In this study, we prepared Pt/Rh/SnO_2 electrocatalysts by the modified Bönnemann method. In addition, EOR activity and durability for the Pt/Rh/SnO_2/CB catalysts were evaluated. The obtained results are summarized as follows.

(1) Pt4f and Sn3d core level spectra of three Pt/Rh/SnO_2/CB catalysts showed that Pt^0, Rh^0 and Sn^{4+} were observed, suggesting that Pt and Rh components were metallic and Sn component was oxidized to SnO_2.
(2) TEM images and XRD patterns of three Pt/Rh/SnO_2/CB catalysts showed that each ternary catalyst was composed of Pt, Rh and/or SnO_2 nanoparticles.
(3) The onset potential of oxidation current for the Pt-65/Rh-10/SnO_2/CB and Pt-56/Rh-19/SnO_2/CB electrodes was ca. 0.2 V vs. RHE which was ca. 0.2 V less positive than that for the Pt/CB electrode.
(4) From CO stripping voltammograms, the shoulder at the lower potential for the three Pt/Rh/SnO_2/CB electrodes was shifted to more positive potentials, suggesting that SnO_2 sites adjacent to Pt atoms which caused the bifunctional effect were decreased.
(5) The oxidation current density at 0.6 V for the each Pt/Rh/SnO_2/CB electrode (ca. 2% h^{-1}) decayed more slowly than that at the Pt-75/SnO_2/CB electrode (ca. 5% h^{-1}).
(6) The main product of EOR at 0.6 V for three Pt/Rh/SnO_2/CB electrodes was acetic acid.

Acknowledgment

This work was partially supported by a Grant-in-Aid for Scientific Research (B), No. 22360310, from the Ministry of Education, Culture, Sports, Science and Technology of Japan.

References

[1] E. Antolini, J. Power Sources 170 (2007) 1.
[2] R.B. Kurtz, B. Braunschweing, P. Mukherjee, R.L. Behrens, D.D. Dlott, A. Wieckowsky, J. Catal. 278 (2011) 181.
[3] S. Rousseau, C. Lamy, E.M. Belgsir, C. Coutanceau, J.M. Léger, Electrochim. Acta 49 (2004) 3901.
[4] A. Kowal, M. Li, M. Shao, K. Sasaki, M.B. Vukmirovic, J. Zhang, N.S. Marinkovic, P. Liu, A.I. Frenkel, R.R. Adzic, Nat. Mater. 8 (2009) 325.
[5] R.S. Ferreira Jr., V.R. Oliveira, R.G.C.S. Reis, G. Maia, G.A. Camara, J. Power Sources 185 (2008) 853.
[6] C. Lamy, A. Lima, V. LeRhun, F. Delime, C. Coutanceau, J.M. Léger, J. Power Sources 105 (2002) 283.
[7] M. Heinen, Z. Jusys, R.J. Behm, J. Phys. Chem. C 114 (2010) 9850.
[8] L. Dubau, F. Hahn, C. Coutanceau, J.M. Léger, C. Lamy, J. Electroanal. Chem. 554–555 (2003) 407.
[9] L. Jiang, G. Sun, Z. Zhou, S. Sun, Q. Wang, S. Yan, H. Li, J. Tian, J. Guo, B. Zhou, Q. Xin, J. Phys. Chem. B 109 (2004) 8774.
[10] F. Vigier, C. Coutanceau, F. Hahn, E.M. Belgsir, C. Lamy, J. Electroanal. Chem. 563 (2004) 81.
[11] H. Wang, Z. Jusys, R.J. Behm, J. Phys. Chem. B 108 (2004) 19413.
[12] H.B. Suffredini, V. Tricoli, L.A. Avaca, N. Vatistas, Electrochem. Commun. 6 (2004) 1025.
[13] Y. Bai, J. Wu, J. Xi, J. Wang, W. Zhu, L. Chen, X. Qiu, Electrochem. Commun. 7 (2005) 1087.
[14] M. González Pereira, M. Dávila Jiménez, M.P. Elizalde, A. Manzo-Robledo, N. Alonso-Vante, Electrochim. Acta 49 (2004) 3917.
[15] J. Ribeiro, D.M. dos Anjos, K.B. Kokoh, C. Coutanceau, J.-M. Léger, P. Olivi, A.R. de Andrade, G. Tremiliosi-Filho, Electrochim. Acta 52 (2007) 6997.
[16] E. Higuchi, K. Miyata, T. Takase, H. Inoue, J. Power Sources 196 (2011) 1730.
[17] J. Thepkaew, S. Therdthianwong, A. Kucernak, A. Therdthianwong, J. Electroanal. Chem. 685 (2012) 41.
[18] M. Ammam, E.B. Easton, J. Power Sources 215 (2012) 188.
[19] S. Mitsushima, T. Takahashi, A. Ariffin, K. Matsuzawa, A. Ishihara, K.-I. Ota, ECS Trans. 16 (2008) 1253.
[20] D.A. Cantane, W.F. Ambrosio, M. Chatenet, F.H.B. Lima, J. Electroanal. Chem. 681 (2012) 56.
[21] E. Higuchi, K. Miyata, H. Inoue, Electrochemistry 78 (2010) 526.
[22] J.P.I. De Souza, S.L. Queiroz, K. Bergamaski, E.R. Gonzalez, F.C. Nart, J. Phys. Chem. B 106 (2002) 9825.
[23] A. Kowal, S.L. Gojkovic, K.S. Lee, P. Olszewski, Y.E. Sung, Electrochem. Commun. 11 (2009) 724.
[24] F. Colmati, E. Antolini, E.R. Gonzalez, J. Alloys Compd. 456 (2008) 264.
[25] H. Bönnemann, P. Britz, W. Vogel, Langmuir 14 (1998) 6654.
[26] J. Cao, C. Du, S.C. Wang, P. Mercier, X. Zhang, H. Yang, D.L. Akins, Electrochem. Commun. 9 (2007) 735.
[27] M. Li, N.S. Marinkovic, K. Sasaki, Electrocatalysis 3 (2012) 376.
[28] K.W. Park, J.H. Choi, B.K. Kwon, S.A. Lee, Y.E. Sung, H.Y. Ha, S.A. Hong, H. Kim, A. Wieckowski, J. Phys. Chem. B 106 (2002) 1869.
[29] J.L. Margitfalvi, I. Bortáth, M. Hegadus, A. Szegedi, Catal. Today 73 (2002) 343.
[30] M. Watanabe, S. Motoo, J. Electroanal. Chem. Interfacial Chem. 60 (1975) 267.
[31] A. Haze, M. Chiku, E. Higuchi, H. Inoue, ECS Trans. 41 (2011) 2277.